



# Optical and structural characterization of aerosol-assisted CVD-grown Ni:ZnO thin films

Krutika Natu<sup>1</sup> · Vipin K. Kaushik<sup>2</sup> · Meena Laad<sup>1</sup>

Received: 10 February 2023 / Revised: 3 April 2023 / Accepted: 6 April 2023 / Published online: 27 April 2023  
© The Korean Physical Society 2023

## Abstract

The present work reports the successful growth and hence, the characterization of Ni:ZnO thin films with varying Ni contents in precursor solution ( $x_{Ni} = 0.0, 0.10, 1.00, 4.84, 9.25$  and  $13.27$  at.%). The thin films were fabricated on soda lime glass substrate. An indigenously designed and developed aerosol-assisted chemical vapor deposition (AACVD) system has been used for the deposition of Ni:ZnO thin film. Zinc acetylacetonate and Nickel acetylacetonate were used as a source material for Zn and Ni, respectively. To prepare liquid precursor, isopropyl alcohol was used as a solvent for zinc acetylacetonate and Nickel acetylacetonate. The deposition was carried out at a constant growth temperature of  $500$  °C with oxygen as a carrier gas for the precursor. Raman spectroscopy, XRD and UV–visible spectroscopy characterizations were performed to investigate the effect of varying  $x_{Ni}$  content over the optical as well as the structural properties of Ni:ZnO thin films. The average transmittance of undoped and Ni-doped ZnO came out to be about  $\geq 95\%$ . The calculated thickness of Ni:ZnO was found to be of the order of hundreds of nanometre i.e., the thin films of sub-micron-sized thickness have been fabricated. The measured bandgaps of Ni:ZnO thin film were found to decrease (red shift) with increasing Ni content in precursor solution. The AACVD-grown Ni:ZnO thin films was found to have low-average absorbance approximately 1% and average reflectance approximately 4%. The XRD characteristic spectra of Ni:ZnO thin films reveal that the required phase is present with a little amount of impurities that matches well with the JCPDS data indicating the hexagonal structure. The particle sizes measured by the XRD Scherer's formula, values of lattice constants and the volume of unit cell of Ni:ZnO were found to be in a good agreement with literature. Raman spectra of pure and Ni-doped ZnO thin films have been measured at room temperature in the wave number range  $150$ – $1300$   $\text{cm}^{-1}$ .  $A_1(\text{TO})$  modes are obtained in the range of  $382$ – $384$   $\text{cm}^{-1}$ . While, the modes obtained in the ranges  $569$ – $572$   $\text{cm}^{-1}$  and  $1098$ – $1104$   $\text{cm}^{-1}$  are allocated as  $A_1(\text{LO})$  and  $A_1(2\text{LO})$  modes respectively.

**Keywords** Aerosol-assisted CVD · Ni:ZnO thin film · Raman spectroscopy · UV–Vis spectroscopy

## 1 Introduction

ZnO has attracted a lot of attention because of its versatility, and it has been made and investigated in a variety of physical forms, including single crystals, thick and thin films, nanostructures etc.[1]. Thin films of ZnO, among other physical forms, have a plethora of very essential uses in electrical and optoelectronic devices, such as photothermal conversion systems [2], transparent conductors[3–5], gas sensors for toxic and combustible gasses [6] and heat mirrors and many others [7]. It is also being looked at as a possible option in emerging fields like spintronics[8]. Ni:ZnO is considered as II-VI diluted magnetic semiconductor material due to its unique magneto-electrical and magnet transport-like properties [9]. However, the mechanism of conductivity change due to Ni incorporation is still inconclusive. The microstructural and

✉ Vipin K. Kaushik  
vip08007@gmail.com

Krutika Natu  
krutikanatu@gmail.com

Meena Laad  
meena@sitpune.edu.in

<sup>1</sup> Department of Applied Science, Symbiosis Institute of Technology (SIT), Symbiosis International (Deemed University) (SIU), Near Lupin Research Park, Lavale, Pune, Maharashtra 412115, India

<sup>2</sup> Department of Applied Physics and Optoelectronics, Shri G.S. Institute of Technology and Science, 23, Sir M. Visvesvaraya Mark, Vallabh Nagar, Indore, Madhya Pradesh 452003, India

optical properties of ZnO are very much sensitive to the method of preparation [10], the type and amount of dopants [11–15]. Thus, fabrication and characterization of doped ZnO thin films via different techniques have attracted considerable attention. NiO has face-centered rhombohedral crystal structure with lattice constants:  $a = 4.17 \text{ \AA}$ ,  $\alpha = 90^\circ 3' 48''$  (at room temperature). NiO can also exhibit small deviations from strict stoichiometry, for example:  $\text{Ni}_{(1-\delta)}\text{O}$ , where  $0 < \delta < 5 \times 10^{-3}$  [16]. The material is opaque and black/brownish when  $\delta$  is close to the upper border, but green and translucent when  $\delta$  is close to zero (usually upon annealing). The resistivity can be reduced via inclusion of  $\text{Ni}^{+2}$  ions either through Ni vacancies or interstitial oxygen sites in NiO crystallites. The actual charge conduction mechanism in nickel oxide is still not clear. Some speculate that it is due to the fact that holes get thermally excited from shallow acceptor levels or there is thermal excitation of polarons (small polaron hopping).

In the past few decades, semiconductor physics has been advanced significantly due to its numerous practical application in the field of research and industry. Materials that preserve their needed qualities under harsh environmental conditions are of great importance. Transparent Conducting Oxides (TCOs) are one of such types of semiconducting materials. TCOs are highly conductive and possess low absorbance in the visible and near-infrared (IR) regions of the electromagnetic spectrum, however, have high UV absorption properties due to their great transparency in the visible area [17]. TCOs are wide band-gap semiconductors that have relatively high free electron concentrations in the conduction band region. The conductivity and mobility of TCOs can be modulated according to the doping concentration that in turn improve transparency and band-gap for TCOs. [17, 18]. TCOs are a compromise between electrical conductivity and optical transmittance for device applications, necessitating careful balancing of these properties. Reduction of the resistivity phenomenon is due to either an increment in the concentration of charge carriers or in the mobility value [19].

Thin-film deposition process is broadly classified into two types of systems—physical vapor deposition (PVD) and chemical vapor deposition (CVD). PVD is a widely used technique for producing high-quality, uniform and adherent thin films of metals and metal oxides, as well as other materials, such as ceramics and polymers. Sputtering and evaporation are examples of PVD techniques that use line-of-sight processes to transfer material from the source to the substrate. This in turn leads to an area-specific deposition of thin film which is directly placed facing the source. Consequently, growth defects are generated, such as pinholes, coating non-uniformity, pores etc. Furthermore, PVD requires higher vacuum conditions as compared to the CVD deposition technique.

Aerosol-Assisted Chemical Vapor Deposition (AACVD) qualifies for uniform, good-quality and high stoichiometric film deposition. The morphology and thickness of film can be deposited by controlling various parameters, such as precursor concentration, deposition and flow rate of the carrier gas [12, 13]. Thus, AACVD has been considered an effective low-cost, sustainable and scalable technique as it requires non-toxic precursors. In the present work, we attempt to deposit Ni-doped and undoped transparent ZnO-based thin films using AACVD method.

As the fabrications of transparent conducting oxide thin films have drawn attention due to their specific electronics and optoelectronics properties, among the various metal oxides, NiO is a p-type semiconductor material, which at room temperature, has a wide band gap of 3.6–4.0 eV. NiO is considered to be optically transparent in the visible light region. It can also be used to fabricate short wavelength optoelectronic devices due to its wide bandgap. NiO is an appealing material because of its excellent optical, magnetic and electrical properties. It is used as an anti-ferromagnetic material for electro-chromic display and a functional layer material in chemical sensors [20]. Optical and electrical properties of Ni-doped ZnO can be connected with its possible applications in today's electronics. Objective of the present project work is the deposition of ZnO and Ni:ZnO thin films using aerosol-assisted CVD system. Structural properties of grown films i.e., phase orientation, grain size and crystalline nature of grown films, were identified by performing X-ray diffraction. Raman spectroscopy was used for the analysis of vibrational modes of Ni:ZnO thin films. Optical transmittance and energy band gap of the AACVD-grown Ni:ZnO thin films were investigated by ultraviolet–visible spectroscopy.

## 2 Results and discussion

The present work is aimed to study the effect of  $\text{Ni}^{+2}$  doping in the lattice of ZnO thin films. The films were created using an aerosol-assisted chemical vapor deposition technique developed in-house. The different mass proportions of zinc acetylacetonate ( $w_1$ ) and nickel acetylacetonate ( $w_2$ ) dissolved in a certain volume of isopropyl alcohol have been used to have various concentrations of precursor. Table 1 shows the experimentally chosen values of fraction of nickel content in precursor solution ( $x_{\text{Ni}}$ ), precursor concentration (PC), deposition time ( $D_t$ ), thickness ( $t$ ), deposition rate ( $D_R$ ) and the optical bandgap ( $E_g$ ) of AACVD-grown Ni:ZnO thin films. To have the precursor with different concentrations, varying mass proportions of nickel acetylacetonate (as given in table 1) have been dissolved in the solution of 200 ml of isopropyl alcohol and 2 g of zinc acetylacetonate.

**Table 1** Experimental parameters of AACVD-grown Ni:ZnO thin films

S	$w_2$	$w_2/w_1$	$x_{Ni}$		PC	$D_t$	$t$	$D_R$	$E_g$
No	g	Ratio	at. %	wt. %	g/l	min	nm	pm/s	eV
1	0.00	–	0.00	0.00	10.00	40	154	64	3.26
2	0.002	1:1000	0.10	0.09	10.01	30	134	74	3.25
3	0.02	1:100	1.00	0.99	10.10	40	185	77	3.24
4	0.1	1:20	4.84	4.76	10.50	32	109	57	3.16
5	0.2	1:10	9.25	9.09	11.00	35	216	103	3.13
6	0.3	3:20	13.27	13.04	11.50	35	209	100	3.10

The values of  $x_{Ni}$  have been calculated in atomic percent (at.%) and weight percent (wt.%). For these calculations, the following expressions have been used:

$$\begin{aligned} x_{Ni} &= (w_1 \times 100)/(w_1 + w_2) \quad (\text{wt.}\%) \\ &= (w_1 \times 100)/(w_1 + w_2 \times C) \quad (\text{at.}\%) \end{aligned} \quad (1)$$

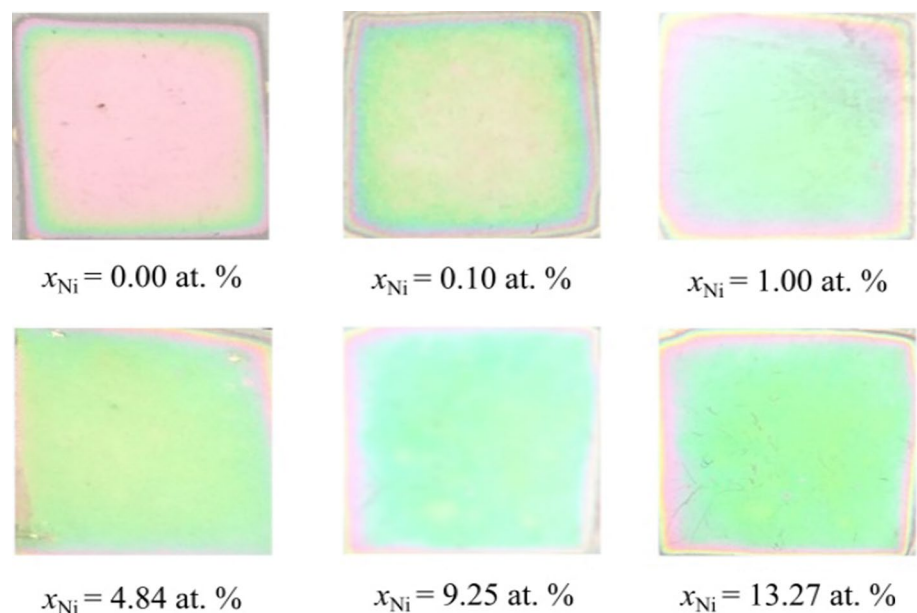
Here,  $C$  is the ratio of molecular weight of nickel acetylacetonate (258.93 amu) to the molecular weight of zinc acetylacetonate (263.61 amu) i.e.,  $258.93/263.61 = 0.98$ . The formula used for the calculation of precursor concentration is  $(w_1 + w_2)/\text{volume of IPA}$ . To calculate the thickness of the present thin films, the density methods have been adopted. The following expression can be used to compute the thickness of the film using this method:

$$t = m_f / (d_f \times A_f) \quad (2)$$

Here,  $m_f$  is the mass,  $d_f$  is the density and  $A_f$  is the surface area of Ni:ZnO thin films. In the present calculations, the density and surface area of AACVD-grown Ni:ZnO thin films were  $5.61 \text{ g/cm}^3$  and  $1 \text{ cm}^2$ , respectively. The masses of the deposited thin films have been calculated by the

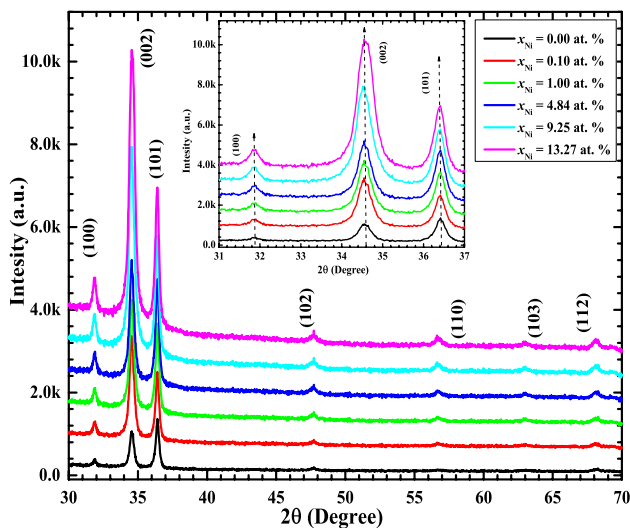
difference of pre- and post-deposition masses of substrate. The calculated values of the thickness of the films have been shown in table 1. These values have further been used to evaluate the rate of deposition  $D_R$  of thin films, which is the ratio of the film thickness and the time of deposition  $D_t$  as given in the table 1. No regular trend has been observed in the deposition rate of AACVD-grown Ni:ZnO thin films because the present AACVD technique relies on the self-assembling of molecules at the heated substrate. The calculated value of average rate of deposition of the films was  $(0.335 \pm 0.030) \text{ nm/s}$ .

Figure 1 shows the pictures of AACVD-grown Ni:ZnO thin films with varying  $x_{Ni}$ . The hue of the current films shows the influence of Ni doping in the lattice of ZnO. As  $x_{Ni}$  increases, the reflection shifts from red wavelength to the green wavelength i.e., blue shift of reflection and hence the red shift of absorption edge or band gap. The same has been confirmed by the optical spectroscopy of the films. The present films have been characterized for their structural and optical properties.

**Fig. 1** Pictorial view of AACVD-grown Ni:ZnO thin films with varying  $x_{Ni}$ 

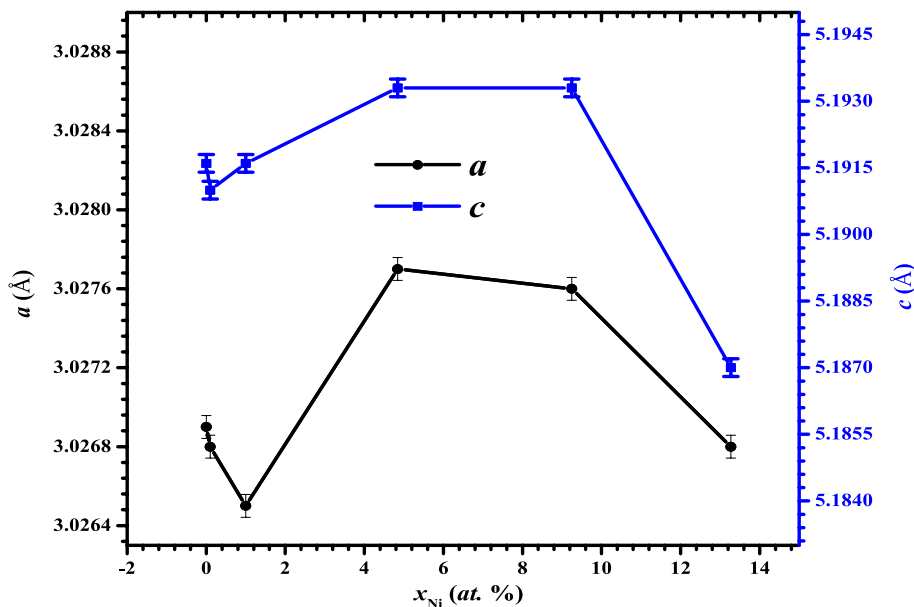
### 3 X-ray diffraction spectroscopy of AACVD-grown Ni:ZnO thin films

X-ray diffraction spectroscopy has been carried out to study the structural properties of the grown films. XRD experiments have been performed at UGC-DAE CSR, Indore using Bruker D8 Advance X-ray diffractometer. Figure 2 shows the XRD pattern of AACVD-grown Ni:ZnO thin films. In this figure, the angle of diffraction ( $2\theta$ ) for a polycrystalline specimen has been plotted as a function of diffracted beam



**Fig. 2**  $\theta$ - $2\theta$  scan of X-ray diffraction pattern of AACVD fabricated Ni:ZnO thin films. The effect of  $x_{Ni}$  over the shift in the position of three prominent peaks (100), (002) and (101) of Ni:ZnO has been highlighted by the inset of the figure

**Fig. 3** Variation of lattice parameters ( $a$  and  $c$ ) of AACVD-grown Ni:ZnO thin films having varying  $x_{Ni}$



intensities where every single peak in the diffraction pattern corresponds to a set of crystallographic planes.

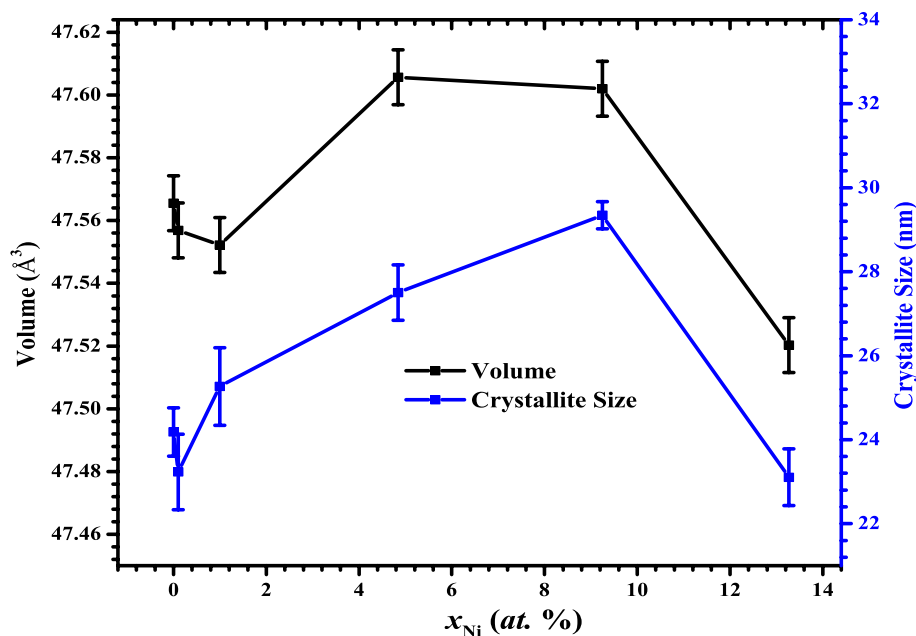
It can be observed that the nature of the films is polycrystalline by the existence of various diffraction peaks. Three well-defined diffraction peaks at (100), (002) and (101), respectively, correlate to the wurtzite (hexagonal) crystalline structure of ZnO in all the samples. These diffraction peaks are in near unison with the conventional value of JCPDS card no. 01-079-2206. The effect of  $x_{Ni}$  over the shift in the position of three prominent peaks (100), (002) and (101) of Ni:ZnO has been highlighted by the inset of figure 2. These three peaks have been used to calculate the lattice constant, lattice volume, crystalline size and the lattice strain of Ni:ZnO thin films. To calculate the lattice parameters ( $a$  and  $c$ ) of Ni:ZnO thin films, the following expression relating Miller indices ( $hkl$ ) and inter-planer spacing ( $d$ ) of the films has been used [21].

$$\frac{1}{d^2} = \frac{4}{3} \left[ \frac{h^2 + hk + k^2}{a^2} + \frac{l^2}{c^2} \right] \tag{3}$$

The calculated values of  $a$  and  $c$  have been further used to calculate the volume of unit cell ( $\sqrt{3}a^2c/2$ ) of hexagonal lattice-structured Ni:ZnO thin films.

The dependance of lattice parameters ( $a$  and  $c$ ) and the volume of unit cell of Ni:ZnO films over the Ni contents  $x_{Ni}$  have been shown by the Figs. 3 and 4, respectively. Although, no regular trend has been found in the variation of lattice parameters ( $a$  and  $c$ ) and the volume of unit cell of Ni:ZnO films, but the variation is small enough to cause the micro-strain in the lattice of ZnO. As demonstrated in the inset of Fig. 2, the distinctive peak of the (002) plane connected to the doped sample shifts toward a higher

**Fig. 4** Variation of volume of unit cell and crystallite size of AACVD-grown Ni:ZnO thin films having varying  $x_{Ni}$



angle when compared to the undoped (pure) ZnO thin film. Aside from this occurrence, we see that the broadening of the XRD peak of Ni-doped samples shows that the size of the doped ZnO thin film is less than the size of the undoped ZnO thin film. The decrease in crystallite size is caused by the entrance of impurities into a host ZnO lattice, and the presence of  $Ni^{+2}$  decreases the nucleation and consequent growth rate of ZnO thin films, as evidenced by oscillations in the rate of growth of samples as shown in Table 1 [22, 23]. A closer look at the XRD spectra indicated that some of the peaks obtained in XRD in doped ZnO thin films at higher angles vanish in pure ZnO samples. This stems from an increase in grain size and the existence of stress/strain in the ZnO lattice caused by the entrance of  $Ni^{+2}$  dopant into the host ZnO lattice. As a result, we infer that tiny changes in  $2\theta$  values of diffraction peaks and the broadening of peak are produced by an increase in micro-strain, and line broadening is mostly the cause of the size and micro-strain of doped ZnO thin films. The following expression depicts the Scherrer's formula to evaluate the average crystalline size.

$$\delta = \frac{0.94\lambda}{\beta \cos\theta} \quad (4)$$

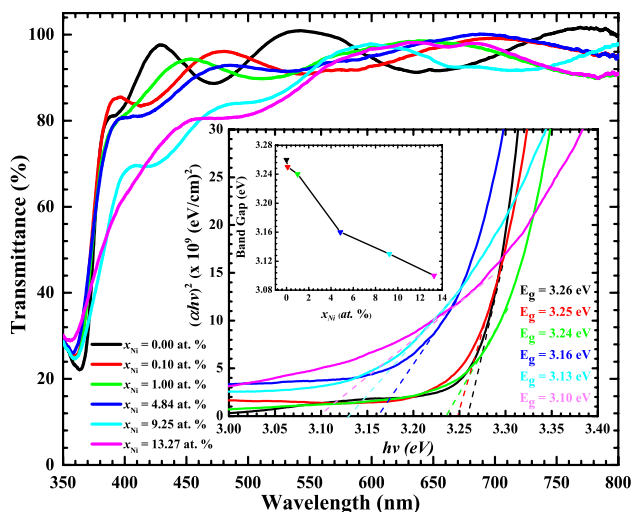
In that equation,  $\delta$  is grain size,  $\lambda$  is the wavelength of X-ray (1.54  $\text{\AA}$ ),  $\beta$  is the full-width at half-maxima, and  $\theta$  is the angle of diffraction.

Fig. 4 shows the variation of crystallite size and the volume of unit cell of AACVD-grown Ni:ZnO thin films having varying Ni contents. It is evident that initially, both the crystallite size and volume of unit cell of Ni:ZnO thin

films increase with increasing  $x_{Ni}$ . For the large amount of doping of  $Ni^{+2}$  ions in the lattice of ZnO, both the crystallite size and volume of unit cell of Ni:ZnO thin films reduce sharply. This is attributed to the limited incorporation of bigger size  $Ni^{+2}$  ion (88  $\text{\AA}$ ) in the lattice site of smaller size  $Zn^{+2}$  ion (74  $\text{\AA}$ ). This introduces an strain in lattice of ZnO and hence the increases in both the crystallite size and volume of unit cell of Ni:ZnO have been observed. On the other hand, the presence of excess of  $Ni^{+2}$  ions hinders the further opening of ZnO that in turn reduces the crystalline size as well as the volume of unit cell of ZnO [23]. The similar behavior in the reduction of band gap of Ni:ZnO has also been observed.

#### 4 Ultraviolet–visible spectroscopy of AACVD-grown Ni:ZnO thin films

Figure 5 depicts the ultraviolet–visible transmittance spectra of AACVD-grown Ni:ZnO thin films having Ni content  $x_{Ni}$  varying from 0.0 to 13.27 at.%. A STDFSM digital fiber spectrophotometer has been used to measure the transmittance spectra from 300 to 800 nm, of Ni:ZnO thin films that are deposited on the glass substrates of soda lime. From the figure, the presence of interference fringes that are clearly noticeable in the visible region of transmission spectra lends credence to the notion that contemporary AACVD-produced Ni:ZnO thin films have optical homogeneity and considerable transmittance. As depicted by figure 5, within the high visible region of 550 to 800 nm, the average optical transmittance ( $T_{Avg}$ ) of Ni:ZnO thin films is  $\approx 90\%$ . For all the films at value  $\geq 380$  nm wavelength, a sharp band edge absorption



**Fig. 5** Ultraviolet-Visible transmittance spectra of AACVD-grown Ni:ZnO thin films having different Ni contents. Inset shows the variation of  $(\alpha hv)^2$  and a function of incident photon energy  $hv$ . The plots are used to calculate the variation of optical band gap  $E_g$  as a function of  $x_{Ni}$  that has also been shown in the inset of figure

has been observed, which corresponds to the optical band gap of undoped as well as doped ZnO.

The absorbance coefficient and band gap energy are connected in the following expression for direct band gap semiconductors, such as pure and doped ZnO.[24]

$$\alpha hv = A(hv - E_g)^{1/2} \quad (5)$$

where  $hv$  is known as incident photon energy,  $E_g$  is the band gap energy and  $A$  is a constant. The variation of  $(\alpha hv)^2$  as a function of incident optical energy  $hv$  has been shown by the inset of Fig. 5 that can be used to determine  $E_g$ . The x-axis intersect of asymptote of  $(\alpha hv)^2$  Vs.  $hv$  curve at  $(\alpha hv)^2 = 0$  directly gives the bandgap of thin film. The variations of calculated bandgap of pure and Ni-doped ZnO have also been plotted in the inset of figure 5. It is interesting to note that with the increase of  $x_{Ni}$ , a monotonically decreasing trend in the bandgap of Ni:ZnO has been observed. This is because with the doping of  $Ni^{2+}$  ions in the lattice of ZnO, the presence of excess  $Ni^{2+}$  ions increases that dominate the bandgap renormalization effect and hence reduce the bandgap of Ni:ZnO as compared to that of ZnO thin film.

The inset of Fig. 5 shows that the bandgap of near band edge UV-Vis spectra decreases with Ni doping, indicating a red shift of the bandgap. Transmittance diminishes as doping concentration increases. This drop in transmittance is caused by the creation of lattice defects as a result of the integration of  $Ni^{2+}$  ion into the host matrix of ZnO. These  $Ni^{2+}$  ions are likely to inhabit the interstitial positions on the ZnO lattice, increasing light absorption and lowering transmission. According to Wakano et al. [25], the transmittance

is affected by surface roughness for the reason that surface scattering brings down transmittance. The almost flat advent of transmittance spectra suggests that the surface is rough, which, thereby, increases surface scattering and thus transmission. With increasing Ni doping concentration, the band-gap values range from 3.26 eV to 3.10 eV. The redshift in energy gap is seen for Ni:ZnO films as Ni content increases are due to exchange in the interaction of p-d pair. Sato et al. [26], have reported that in Ni:ZnO, half-metallic behavior exists, and magnetic impurities of d states generally turn up near the Fermi level. Furthermore, the XRD spectrum analysis confirms the hypothesis that  $Ni^{2+}$  ions replace  $Zn^{2+}$  ions in the tetrahedron's center. Due to the impact of the ZnO tetrahedral crystal field, the d electronic states in this field split into lower doublet states and higher energy triplet levels. The triplet states hybridize with the valence band's p orbitals, resulting in bonding as well as anti-bonding states. Also, these states are located inside the band gap, such as the bonding states are closer to the valence band and anti-bonding states, having higher energy, are close to the conduction band. As a result, a red shift occurs due to the optical absorption between these states. Additionally, the possibility of the reduction in band gap as a result of rise in crystalline nature with increasing  $x_{Ni}$  of the films can be ruled out by the presence of number of XRD peaks that supports the polycrystalline nature of AACVD-grown Ni:ZnO thin films [27].

The STDFSM digital fiber spectrophotometer can also be used to measure the optical absorbance and reflectance of thin film. Figure 6a and 6b shows the optical absorbance and reflectance spectra of AACVD-grown Ni:ZnO thin films having different Ni contents. It is worthy to note that all the films have low-average optical absorbance  $\leq 1\%$  and considerably low-average optical reflectance  $\leq 4\%$ . From the absorption spectra, it can be seen that the absorption peak of undoped and Ni-doped ZnO appear from  $\approx 380$  nm. Furthermore, with the increase of nickel concentration, the absorption peak of Ni:ZnO thin films becomes broad.

## 5 Raman spectroscopy

Raman spectroscopy is considered as one of the dominant tools in order to identify the presence of dopants and lattice defects in the lattice structure of the host element. The transport of charges within the dopant and host material modifies the surface of doped thin films resulting in the shift in the optical Raman spectrum of doped and un-doped thin films. Figure 7 depicts the Raman spectra of pure and Ni-doped ZnO thin films measured at room temperature in the wavenumber range  $150-1300$   $cm^{-1}$ .

In the ZnO wurtzite structure, all atoms occupy the  $C_{4v}$  sites, and there are two formulae units per primitive cell. The group theory ( $A_1+2B_1+E_1+E_2$ ) predicts both the

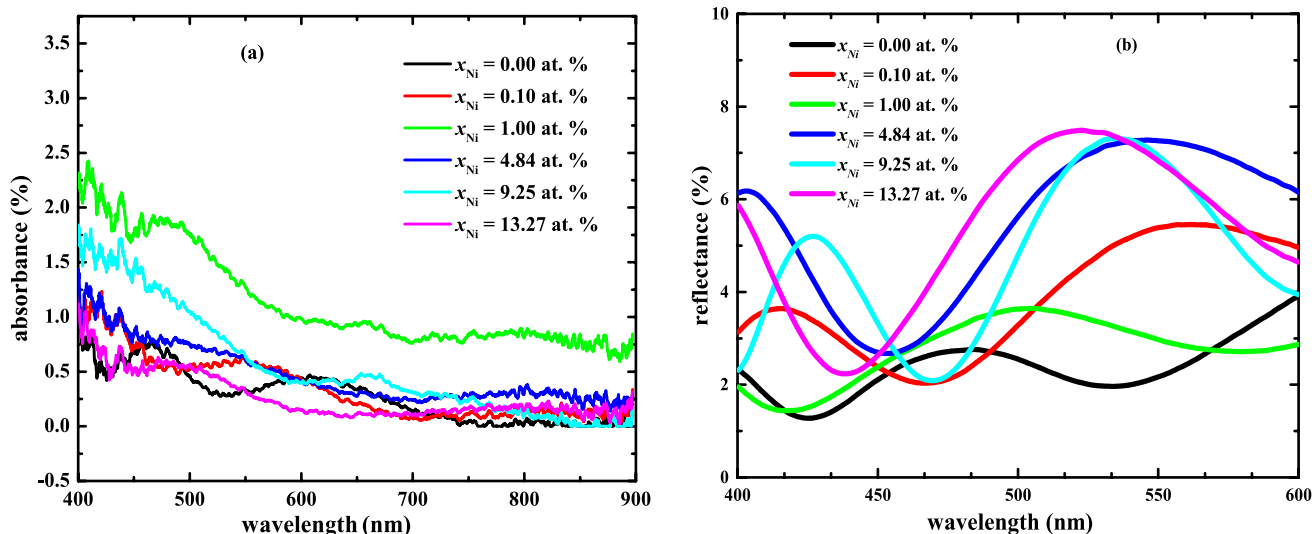


**Fig. 6** Optical **a** absorbance and **b** reflectance of AACVD-grown Ni:ZnO thin films having different Ni contents

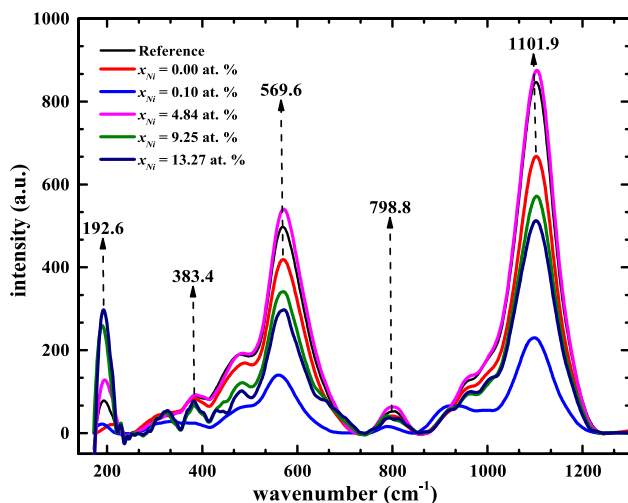


**Fig. 7** Raman spectra of AACVD-grown Ni:ZnO thin films having different Ni contents

Raman-active center and optical phonons. As they are polar phonons, the transverse optical (TO) and longitudinal optical (LO) phonons of the symmetry  $A_1$  and  $E_1$  exhibit distinct frequencies with being Raman and infrared active.  $B_1$  modes are Raman-inactive or silent modes. Moreover,  $E_2$  modes are non-polar, but Raman-active modes. The peaks obtained for pure and doped ZnO thin films in the range of  $382\text{--}384\text{ cm}^{-1}$  are attributed as  $A_1(\text{TO})$  transverse optical mode and those in the range of  $569\text{--}572\text{ cm}^{-1}$  are  $A_1(\text{LO})$  mode due to the presence of oxygen vacancies, Zn interstitials or free carriers in the films. Peaks in the range of  $1098\text{--}1104\text{ cm}^{-1}$  are allocated as the second-order vibrational mode  $A_1(2\text{LO})$  [28–31]. After Ni doping, a shift in peak width and

frequency is seen, which may indicate a change in local symmetry as a result of the inclusion of Ni atoms in the host lattice even while the crystal structure is unaltered. Also an additional mode has been observed in doped ZnO thin films at  $192.6\text{ cm}^{-1}$ . However, the reason for the peak is still unclear as there has been some dissimilar reasoning in the previous literature [29]. To peaks at  $788\text{--}800\text{ cm}^{-1}$ , an additional mode is assigned to be longitudinal optical and longitudinal acoustic modes as  $A_1(\text{LA}+\text{LO})$  that are related to glass substrate.

## 6 Conclusions

In summary, the present work can be concluded with the findings as, Ni:ZnO thin films having various Ni contents  $x_{\text{Ni}}$ , have been deposited on soda lime glass substrate kept at constant growth temperature of  $500\text{ }^\circ\text{C}$ . The Raman spectroscopy, XRD and UV–visible spectroscopy characterizations were performed to investigate the effect of varying  $x_{\text{Ni}}$  over the optical as well as structural properties of the deposited Ni:ZnO thin films. Furthermore, the XRD characterization of Ni:ZnO thin films reveals that the required phase is present with a little amount of impurities that matches well with the with JCPDS data indicating the hexagonal structure. The particle sizes measured by the XRD Scherer's formula, values lattice constants and the volume of unit cell of Ni:ZnO were found to be in a good agreement with literature. The UV–Vis spectroscopy of grown films shows that the deposited films were highly transparent in the region of visible spectra. The optical band gap decreases evidently as dopant concentration increases, indicating that Ni doping favorably narrows the band gap of ZnO. The AACVD-grown Ni:ZnO

thin films were found to have low-average absorbance  $\approx 1\%$  and average reflectance  $\approx 4\%$ . Additionally, Raman spectroscopy of the films shows the presence of various vibrational modes like first- and second-order vibration modes, optical mode (transverse) and the optical phonon mode (longitudinal). The doping of Ni<sup>2+</sup> ions in the lattice of ZnO showed shift in the local symmetry by the change in peak width and frequency. Ni doping could be studied to have highly stable and conductive p-type Ni:ZnO thin films. Post-deposition annealing of Ni:ZnO thin films could also be explored to get the best p-type conductivity and transparency of AACVD-grown Ni:ZnO thin films.

**Acknowledgements** The authors acknowledge Dr. J.T. Andrews of SGSITS Indore, for the constant guidance and support during the course of the work. The authors also thank Dr. Mukul Gupta for XRD characterization at UGC-DAE CSR, Indore.

**Author Contributions** All authors contributed to the study conception and design. Material preparation, data collection and analysis were performed by Krutika Natu and Vipin K. Kaushik. The first draft of the manuscript was written by Vipin K. Kaushik, and Meena Laad and all authors commented on previous versions of the manuscript. All authors read and approved the final manuscript.

**Funding** The authors declare that no funds, grants, or other support was received during the preparation of this manuscript.

**Data availability** The raw/processed data required to reproduce these findings cannot be shared at this time as the data also forms part of an ongoing study.

## Declarations

**Conflict of interest** The authors have no relevant financial or non-financial interests to disclose.

## References

1. Y. Liu, Y. Li, H. Zeng, ZnO-based transparent conductive thin films: Doping, performance, and processing. *J. Nanomater.* **2013**, 1–9 (2013). <https://doi.org/10.1155/2013/196521>
2. J. Fang, Y. Xuan, Investigation of optical absorption and photo-thermal conversion characteristics of binary CuO/ZnO nanofluids. *RSC Advanc.* **7**(88), 56023–56033 (2017). <https://doi.org/10.1039/c7ra12022b>
3. C.-Y. Wu, L.-C. Chiu, J.-Y. Juang, High haze Ga and Zr co-doped zinc oxide transparent electrodes for photovoltaic applications. *J. Alloys Compounds* **901**, 163678 (2022). <https://doi.org/10.1016/j.jallcom.2022.163678>
4. R. Liu, Y. Chen, S. Ding, Y. Li, Y. Tian, Preparation of highly transparent conductive aluminum-doped zinc oxide thin films using a low-temperature aqueous solution process for thin-film solar cells applications. *Solar Energy Mater. Solar Cells* **203**, 110161 (2019). <https://doi.org/10.1016/j.solmat.2019.110161>
5. S.D. Ponja, S. Sathasivam, I.P. Parkin, C.J. Carmalt, Highly conductive and transparent gallium doped zinc oxide thin films via chemical vapor deposition. *Scientific* (2020). <https://doi.org/10.1038/s41598-020-57532-7>
6. G. Biasotto, M.G.A. Ranieri, C.R. Foschini, A.Z. Simões, E. Longo, M.A. Zaghete, Gas sensor applications of zinc oxide thin film grown by the polymeric precursor method. *Ceramics* (2014). <https://doi.org/10.1016/j.ceramint.2014.06.099>
7. A. Eshaghi, A. Graeli, M. Hajkarimi, Fabrication of transparent conductive aluminum zinc oxide nanostructured thin film on polycarbonate substrate for heat mirror applications. *Journal of Optical Technology.* **82**(1), 51 (2015).
8. K. Jeyasubramanian, Rv. William, P. Thiruramanathan, G.S. Hikku, M. Vimal Kumar, B. Ashima, P. Veluswamy, H. Ikeda, Dielectric and magnetic properties of nanoporous nickel doped zinc oxide for spintronic applications. *J. Magnet. Magnet. Mater.* **485**, 27–35 (2019). <https://doi.org/10.1016/j.jmmm.2019.04.032>
9. A. Samanta, M.N. Goswami, P.K. Mahapatra, Magnetic and electric properties of Ni-doped ZnO nanoparticles exhibit diluted magnetic semiconductor in nature. *J. Alloys Compounds* **730**, 399–407 (2018). <https://doi.org/10.1016/j.jallcom.2017.09.334>
10. S. Sánchez-Martín et al., Study of deposition parameters and growth kinetics of ZnO deposited by aerosol assisted chemical vapor deposition. *RSC Advanc.* **11**(30), 18493–18499 (2021). <https://doi.org/10.1039/d1ra03251h>
11. D. Viet Vu, D. Hai Le, C. Xuan Nguyen, T. Quang Trinh, Comparison of structural and electric properties of ZnO-based N-type thin films with different dopants for thermoelectric applications. *J. Sol-Gel Sci. Technol.* **91**(1), 146–153 (2019). <https://doi.org/10.1007/s10971-019-05024-0>
12. A. Jiamprasertboon et al., Low-cost one-step fabrication of highly conductive ZnO: Cl transparent thin films with tunable photocatalytic properties via aerosol-assisted chemical vapor deposition. *ACS Appl. Electron. Mater.* **1**(8), 1408–1417 (2019). <https://doi.org/10.1021/acsaem.9b00190>
13. Z. Manzoor, et al. (2020) “Optical and structural properties of nickel doped zinc oxide grown by metal organic chemical vapor deposition (MOCVD) at different reaction chamber condition.” *ES Materials & Manufacturing [Preprint]*. 10.30919/esmm5f715
14. Ö. Çelik, Ş Baturay, Y.S. Ocağ, Sb doping influence on structural properties of ZnO thin films. *Mater. Res. Exp.* **7**(2), 026403 (2020). <https://doi.org/10.1088/2053-1591/ab6c8a>
15. J. Mathew, G. Varghese, J. Mathew. 2014 “Structural and optical properties of Ni:ZnO thin films-effect of annealing and doping concentration.” *SOP Transactions on Applied Physics*. 10.15764/aphy.2014.04003
16. C.C. Diao, C.Y. Huang, C.F. Yang, C.C. Wu, Morphological, optical, and electrical properties of P-type nickel oxide thin films by nonvacuum deposition. *Nanomaterials* **10**(4), 636 (2020). <https://doi.org/10.3390/nano10040636>
17. D.B. Potter et al., Al-, Ga-, and In-doped ZnO thin films via aerosol assisted CVD for use as transparent conducting oxides. *Phys. Status Solidi.* **213**(5), 1346–1352 (2016)
18. J.A. Spencer, A.L. Mock, A.G. Jacobs, M. Schubert, Y. Zhang, M.J. Tadjer, A review of band structure and material properties of transparent conducting and semiconducting oxides: Ga<sub>2</sub>O<sub>3</sub>, Al<sub>2</sub>O<sub>3</sub>, In<sub>2</sub>O<sub>3</sub>, ZnO, SnO<sub>2</sub>, CdO, NiO, CuO, and Sc<sub>2</sub>O<sub>3</sub>. *Appl. Phys. Rev.* **9**(1), 011315 (2022). <https://doi.org/10.1063/5.0078037>
19. A. de Andres, F. Jimenez-Villacorta, C. Prieto, The compromise between conductivity and transparency. *Trans. Conduct. Mater.* (2018). <https://doi.org/10.1002/9783527804603.ch1>
20. Sani Garba Danjuma, Nickel oxide (NiO) devices and applications: a review. *Int. J. Eng. Res.* (2019). <https://doi.org/10.17577/ijertv8is040281>
21. I. Elhamdi, H. Souissi, O. Taktak, J. Elghoul, S. Kammoun, E. Dhahri, B.F. Costa, Experimental and Modeling Study of ZnO: Ni nanoparticles for near-infrared light emitting diodes. *RSC Advanc.* **12**(21), 13074–13086 (2022). <https://doi.org/10.1039/d2ra00452f>
22. M.Y. Ali, M.K.R. Khan, A.T. Karim, M.M. Rahman, M. Kamruzzaman, Effect of Ni doping on structure, morphology and



- opto-transport properties of spray pyrolysed ZnO nano-fiber. *Heliyon* (2020). <https://doi.org/10.1016/j.heliyon.2020.e03588>
23. T.V.K. Karthik, M.D.L.L. Olvera, A. Maldonado, R.R. Biswal, H. Gómez-Pozos, Undoped and nickel-doped zinc oxide thin films deposited by DIP coating and ultrasonic spray pyrolysis methods for propane and carbon monoxide sensing applications. *Sensors* **20**(23), 6879 (2020). <https://doi.org/10.3390/s20236879>
  24. O. Bayram, E. Sener, E. İgman, O. Simsek, Investigation of structural, morphological and optical properties of nickel-doped zinc oxide thin films fabricated by co-sputtering. *J. Mater. Sci. Mater. Electron.* **30**(4), 3452–3458 (2019). <https://doi.org/10.1007/s10854-018-00620-2>
  25. T. Wakano, N. Fujimura, Y. Morinaga, N. Abe, A. Ashida, T. Ito, Magnetic and Magneto-transport properties of ZnO: Ni films. *Phys. E Low-Dimension. Syst. Nanostruct.* **10**(1–3), 260–264 (2001). [https://doi.org/10.1016/s1386-9477\(01\)00095-9](https://doi.org/10.1016/s1386-9477(01)00095-9)
  26. K.S. Kazunori Sato, H.K.-Y. Hiroshi Katayama-Yoshida, Material design for transparent ferromagnets with ZnO-based magnetic semiconductors. *Japanese Journal of Applied Physics.* (2000). <https://doi.org/10.1143/jjap.39.1555>
  27. S.B. Rana, R.P. Singh, Investigation of structural, optical, magnetic properties and antibacterial activity of Ni-doped zinc oxide nanoparticles. *J. Mater. Sci. Mater. Electron.* **27**(9), 9346–9355 (2016)
  28. R. Siddheswaran, M. Netrvalová, J. Savková, P. Novák, J. Očenášek, P. Šutta, R. Jayavel, Reactive magnetron sputtering of Ni doped ZnO thin film: Investigation of Optical, structural, mechanical and magnetic properties. *J. Alloys Compounds* **636**, 85–92 (2015). <https://doi.org/10.1016/j.jallcom.2015.02.142>
  29. A.K. Rana, Y. Kumar, P. Rajput, S.N. Jha, D. Bhattacharyya, P.M. Shirage, Search for origin of room temperature ferromagnetism properties in Ni-doped ZnO nanostructure. *ACS Appl. Mater. Interf.* **9**(8), 7691–7700 (2017). <https://doi.org/10.1021/acsami.6b12616>
  30. M. Koyano, P. QuocBao, L.T. ThanhBinh, L. HongHa, N. Ngoc-Long, S.I. Katayama, Photoluminescence and Raman spectra of ZnO thin films by charged liquid cluster beam technique. *Phys. Status Solidi.* **193**(1), 125–131 (2002)
  31. P. Kaim, K. Lukaszkwicz, M. Szindler, M. M. Szindler, M. Basiaga, B. Hajduk, The influence of magnetron sputtering process temperature on ZnO thin-film properties. *Coatings* **11**(12), 1507 (2021). <https://doi.org/10.3390/coatings11121507>

**Publisher's Note** Springer Nature remains neutral with regard to jurisdictional claims in published maps and institutional affiliations.

Springer Nature or its licensor (e.g. a society or other partner) holds exclusive rights to this article under a publishing agreement with the author(s) or other rightsholder(s); author self-archiving of the accepted manuscript version of this article is solely governed by the terms of such publishing agreement and applicable law.